Forensic Science International 208 (2011) 156–166

Contents lists available at ScienceDirect

Forensic Science International

journal homepage: www.elsevier.com/locate/forsciint

Temporal variation of oxygen isotope ratios ($\delta^{18}O$) in drinking water: Implications for specifying location of origin with human scalp hair

Casey D. Kennedy [a,*], Gabriel J. Bowen [a,b], James R. Ehleringer [c,d]

[a] Purdue University, Department of Earth and Atmospheric Sciences, 550 Stadium Mall Drive, West Lafayette, IN 47907-2051, USA
[b] Purdue Climate Change Research Center, Purdue University, 550 Stadium Mall Drive, West Lafayette, IN 47907-2051, USA
[c] Department of Biology, University of Utah, Salt Lake City, UT 84112, USA
[d] IsoForensics, Inc., Salt Lake City, UT 84108, USA

ARTICLE INFO

Article history:
Received 25 August 2010
Received in revised form 16 November 2010
Accepted 23 November 2010
Available online 21 February 2011

Keywords:
Isotope geochemistry
Human provenance
Uncertainty
Region of origin
Hair
Bayesian

ABSTRACT

Previous work suggests that $\delta^{18}O$ values of human hair can be used to constrain the region-of-origin of unknown individuals, but robust assessments of uncertainties in this method are lacking. Here we assess one source of uncertainty – temporal variation in the $\delta^{18}O$ value of drinking water – using a monthly tap water survey of $\delta^{18}O$ to develop geospatial models (i.e., maps) of the intra-annual variation (seasonality) in tap water $\delta^{18}O$ for the contiguous USA. Temporal variation in tap water $\delta^{18}O$ was correlated with water-supply type, and was related to geographic patterns of precipitation $\delta^{18}O$ seasonality and water residence time. The maps were applied in a Bayesian framework to identify the geographic origin of an unidentified woman found in Utah, based on measured $\delta^{18}O$ of scalp hair. The results are robust in specifying parts of the western USA as the most likely region-of-origin. Incorporation of tap water $\delta^{18}O$ seasonality in the analysis reduces the precision of geographic assignments, but other sources of uncertainty (e.g., spatial interpolation uncertainty) have an equal or larger effect.

1. Introduction

Stable isotopes of hydrogen (^{1}H and ^{2}H) and oxygen (^{16}O and ^{18}O) in human drinking water vary widely in space and time, mainly as a result of the partitioning of heavy and light isotopes in precipitation during phase-change reactions in the hydrological cycle. The primary driver of the systematic geospatial patterns of H and O isotope ratios in precipitation is the preferential stripping of the heavy isotopes (i.e., ^{2}H and ^{18}O) from water vapor as ocean-saturated air masses move inland and across continents. This progressive rainout process is at the root of much of the geographic variation in precipitation isotopes, and is largely dependent on changes in air mass temperature and pressures via their effect on saturation vapor pressure. At global to regional scales, the spatial variation in the isotopic composition of environmental water resources (e.g., lakes, rivers, and groundwater) and human drinking water is consistent with the geographic patterns of precipitation isotopes, modified locally in some cases by isotope effects associated with post-precipitation evaporative loss [1–5].

Spatially explicit patterns of H and O isotopes in human drinking water [1] are preserved in biological materials such as human scalp hair [6], but other factors, such as the dietary inputs to an individual consumer, may also influence the geospatial variation in H and O isotope values of hair. However, the specific impact of variable dietary inputs among consumers on the geographic assignment of human hair may be moderated by the observation that the isotopic composition of local tap water is a reasonable proxy for many beverages, including bottled water [7,8], soda [8], and milk [9]. In spite of these limitations, the application of stable isotope ratios of H and O in human hair to distinguish individuals of different geographic origins has featured prominently in the literature [6,10–14] and has provided valuable information in cases involving the identification of human remains [15,16]. Common statistical methods for estimating the geographic origin of individuals using stable isotopes range in complexity from simple classification trees to computationally intensive hierarchal models of stochastic error processes [17], and (at least with respect to the evaluation of forensic evidence) commonly involve estimating the probability (or likelihood) that the isotopic values characteristic of a specific region are consistent with the measured isotope ratio in a sample (e.g., gathered from a crime scene). One approach, described in [18], exploits the use of spatially continuous models within a Bayesian probabilistic framework to yield the likelihood that any point in space is the "true" origin of an individual for which H or O isotope ratios have been measured. A key advantage of this method is that it is not limited to binary results (ones or zeros), but rather discloses the

* Corresponding author. Tel.: +1 7654963460.
E-mail addresses: cdkennedy@purdue.edu (C.D. Kennedy), gabe@purdue.edu (G.J. Bowen), jim.ehleringer@utah.edu (J.R. Ehleringer).

0379-0738/$ – see front matter © 2010 Elsevier Ireland Ltd. All rights reserved.
doi:10.1016/j.forsciint.2010.11.021

universe of possible outcomes based on estimable sources of uncertainty [17].

The development of stable isotope forensics of human hair is advancing in parallel with closely related applications involving the H and O isotopic composition of organic tissues in wildlife forensics [19–22]. Specifically, a large amount of work has focused on the use of isotope ratios of bird feathers to reconstruct patterns of avian migration, and many of the statistical methods used in the study of migratory birds can be applied to forensic investigations invoking O isotope ratios in human scalp hair. For example, several studies have evaluated the individual or combined effects of analytical measurement error, population variance, or spatial interpolation error on the isotope-based assignment of breeding origin of migratory birds [18,22–27], but comparable statistical considerations of uncertainly in the geographic assignment of human hair are lacking. Because many body tissues such as hair incorporate isotopes from the environment during a short period of growth, and the timing of growth may not always be known, one potential source of uncertainty in the interpretation of hair isotope ratios is the temporal (both seasonal and inter-annual) isotopic variation in drinking water ingested by individuals. In this study, we use a dataset documenting the spatiotemporal variation in $\delta^{18}O$ values of tap water to (1) develop geospatial representations of temporal variation in $\delta^{18}O$ values of tap water and (2) explore the effects of temporal variation in $\delta^{18}O$ values of tap water on the geographic assignment of scalp hair from the decomposed remains of a woman found in a Utah (USA) desert. As a point of comparison, we also analyze how geographic assignment of hair is affected by spatial interpolation uncertainty, which we define as the uncertainty that arises from interpolation of point values used to create maps of $\delta^{18}O$ in tap water (e.g., [1]). Assignment results are presented as the geographic distribution of likelihood values across the contiguous USA, following the methods of [18].

2. Methods

2.1. Data and analysis

Our analysis of temporal variation was based on a 2-year-long monthly survey of stable isotope ratios of O and H in human drinking water from 45 sites across the USA and 1 southern province in Canada (Fig. 1, Table 1). All data are reported as δ values (where $\delta = R_{sample}/R_{standard} - 1$, $R = {}^{18}O/{}^{16}O$ or ${}^{2}H/{}^{1}H$) and normalized on the VSMOW–VSLAP reference scale through repeated analysis of 2 calibrated laboratory reference waters [28]. Analytical methods consisted of injecting a single small (1 mL) aliquot of water onto a column of glassy carbon held at 1400 °C to produce H_2 and CO gases. These were separated chromatographically in a helium carrier gas stream and introduced sequentially into the ion source of an IRMS (Delta +XL, ThermoFinnigan) for isotope ratio determination. Samples were analyzed in duplicate, with average precision of 1.5% for δ^2H and 0.2% for $\delta^{18}O$ (1 standard deviation) for replicate analyses.

The analysis reported here focuses on $\delta^{18}O$ values of tap water, for which 918 samples were obtained (21–24 monthly samples at 30 sites and 9–20 monthly samples at the remaining 15 sites). Based on information collected from individuals and public supply water companies, water supplies for the 45 sites were classified into 3 groups: groundwater (16 sites), surface water (20 sites), or "managed water" (9 sites), which consist either of groundwater–surface water mixtures that fluctuate seasonally in response to changes in water supplies and demands or imported water from one or more non-local sources. Tap water values were compared with $\delta^{18}O$ values of precipitation at the sampling sites as estimated based on geostatistical interpolation of a global precipitation isotope database using the Online Isotopes in Precipitation Calculator (OIPC, http://waterisotopes.org, accessed January 2010; [29,30]). Briefly, this tool allows for calculation of long-term average monthly precipitation $\delta^{18}O$ and δ^2H at specified locations through geostatistical modeling of precipitation isotope data covering the time period 1960–2004 [29–31]. The precipitation model for $\delta^{18}O$ and δ^2H exhibits relatively strong predictive accuracy in most parts of the contiguous USA (average 2 standard deviation uncertainty of modeled mean annual δ^2H is ~8‰ and $\delta^{18}O$ is ~1.0‰, see [29]), with significant exceptions occurring along the Pacific coast in northern California and Oregon where sparse sampling does not adequately capture the strong isotopic gradients known to exist between coastal and inland regions [32].

Temporal variation of tap water $\delta^{18}O$ values was evaluated as (1) inter-annual range, (2) intra-annual range, and (3) standard deviation (σ_{TAP}). Inter-annual range was calculated as the difference in mean annual $\delta^{18}O$ for years 2005 and 2006 for the 31 sites having 9 or more monthly values in both sampling years. Intra-annual range was calculated as the range of monthly average values. Values of σ_{TAP} were calculated from all available tap water measurements, and compared with the standard deviation of monthly amount-weighted precipitation $\delta^{18}O$ (σ_{PPT}):

$$\sigma_{PPT} = \sqrt{\frac{\sum_{j=1}^{12} w_j (x_j - \bar{x})^2}{\left(12 - 1\sum_{j=1}^{12} w_j\right)/12}} \quad (1)$$

where $\bar{x}$ is the OIPC-calculated estimate of the mean annual amount-weighted $\delta^{18}O$ in precipitation, x_j is the 12 monthly averaged precipitation $\delta^{18}O$ estimates, weighted by long-term (1971–2000) monthly precipitation ($w_j = P_j / \sum_{j=1}^{12} P_j$, where values of P_j are precipitation amounts obtained from the PRISM Climate Group, Oregon State University, http://www.prismclimate.org, accessed March 2010).

Maps of both temporal variation and spatial interpolation uncertainty in $\delta^{18}O$ values of tap water were created using geostatistical modeling (see Sections 3.2 and 3.3) and data interpolation by ordinary kriging. All statistical and geostatistical calculations were carried out in Microsoft Excel 2007 and ArcGIS 9.3 (Geostatistical Analyst extension). Map calculations were performed using the USA contiguous states Albers equal area conic projection and a grid size of 263 km^2 (map area = 9,855,138 km^2). Autocorrelation was quantified using Morans I and unstandardized weights derived from squared inverse Euclidean distances between data points. We compare the resulting maps with a map representing the uncertainty of the predicted mean tap water isotope ratio values, another independent source of uncertainty in map-based geographic region-of-origin predictions. In the case of the USA tap water maps used here, uncertainty can be estimated analytically from the properties of the semivariogram model used in geostatistical interpolation (Kriging) of the tap water map [1,33]. A map of the standard error of mean tap water $\delta^{18}O$ predictions (referred to hereafter as "spatial interpolation uncertainty") was calculated in ArcGIS 9.3 using the Geostatistical Analyst extension.

2.2. Geographic assignment

The maps of temporal variation and spatial interpolation uncertainty were incorporated in a suite of analyses to examine the effects of different sources of uncertainty on likelihood of origin estimates based on human hair $\delta^{18}O$ values. As described in [18], likelihood values of "true" geographic origin can be cast within a Bayesian probabilistic framework (e.g., Refs. [22,27]):

$$P(A_i|B) = \frac{P(B|A_i)P(A_i)}{\sum_i P(B|A_i)P(A_i)}, \quad (2)$$

where $P(A_i|B)$ is the "posterior" probability distribution of the observed hair sample value B having originated in geolocation i with predicted $\delta^{18}O$ value A_i. $P(B|A_i)$ is the "likelihood" probability distribution of obtaining the measured $\delta^{18}O$ value in the hair sample, given the modeled distribution of $\delta^{18}O$ values at geographic location i. $P(A_i)$ is the "prior" probability distribution, based on assumptions or evidence that informs geographic assignment in the absence of measured of modeled values of $\delta^{18}O$. The denominator, $\sum_i P(B|A_i)P(A_i)$ (traditionally expressed as $P(B)$ and referred to as the prior probability on B), is a normalizing constant that, in our analysis, is spatial invariant.

Because our primary objective was to isolate the influence imparted by temporal variation and interpolation uncertainty on geographic assignment, we used a flat (or uniform) prior probability equal to 1 for the contiguous USA, and assumed a value of zero for all locations outside of this range (e.g., [27]). For the contiguous USA, and assuming a normal probability distribution, Eq. (2) reduces to the likelihood term:

$$P(A_i|B) \approx L(y|\mu_i, \sigma_i^2) = \frac{1}{\sqrt{2\pi\sigma_i^2}} e^{-(y-\mu_i)^2/2\sigma_i^2} \quad (3)$$

where L is the likelihood that the isotopic composition of y is derived from a geographic location i with modeled values μ_i and σ_i. Values of μ_i were calculated using the empirically derived relationship between $\delta^{18}O$ in hair and tap water: $\mu_i = 0.353\delta^{18}O + 15.2‰$ [6], assuming no uncertainty associated with this transformation and using the geographic distributions of tap water $\delta^{18}O$ in [1]. Although this assumption is clearly inappropriate for real-world applications of the method, it again allows us to focus our analysis on the uncertainty associated with specific variables. Different factors contributing to σ_i have been evaluated for the geographic assignment of migratory birds (e.g., [18,22,24–27]), with the vast majority of these studies structuring σ_i as either the standard deviation about the population mean or the error in predicted values of μ_i. In our analysis, we consider the component contributions of σ_i arising from temporal variation and spatial interpolation uncertainty in tap water values of $\delta^{18}O$ (σ_{TAP} and σ_{TAP}^*, respectively), scaling each of these values by the hair/water regression model coefficient 0.353 [6].

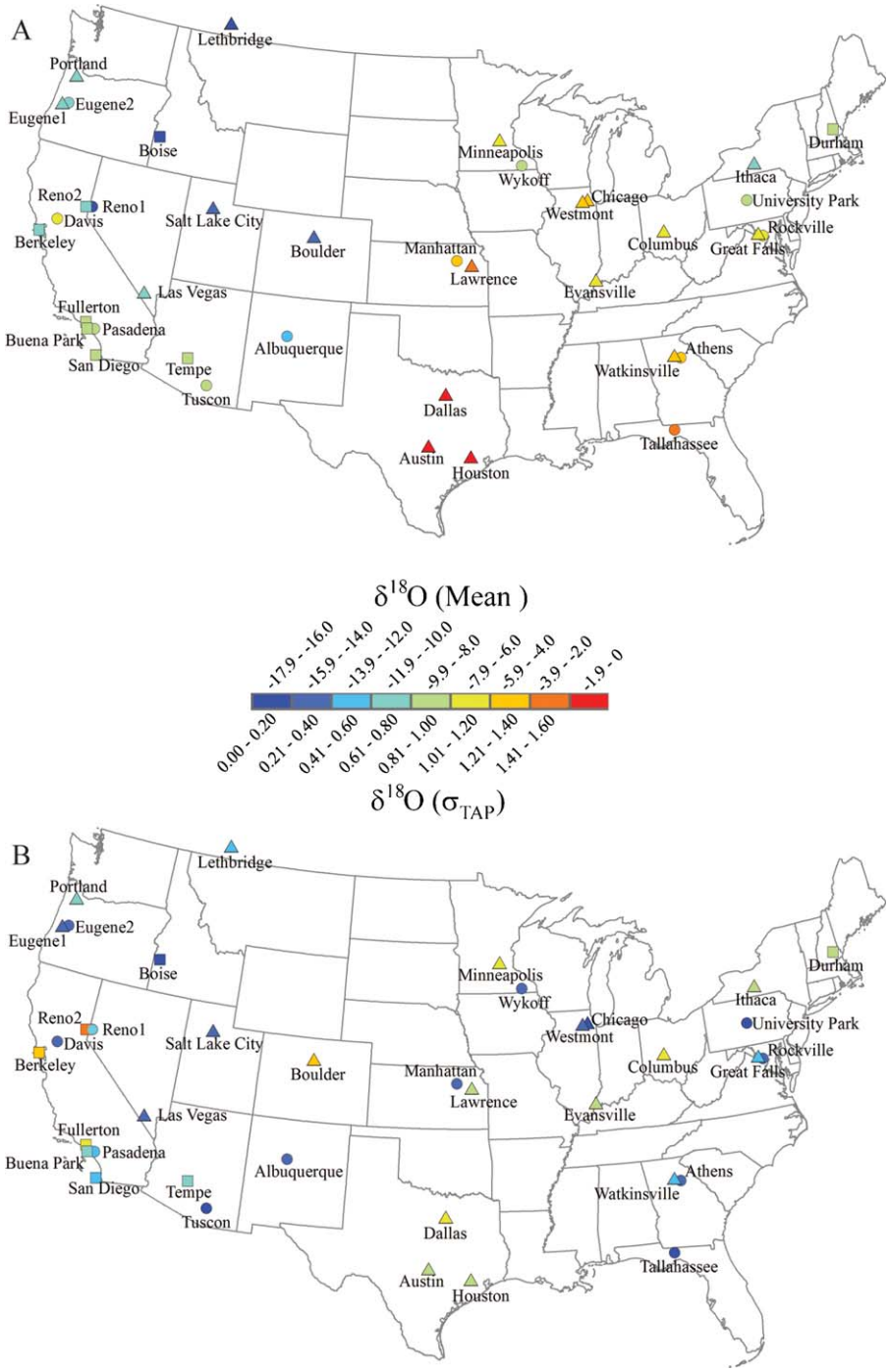

Fig. 1. $\delta^{18}O$ values of tap water from a 2-year monitoring effort at 45 sites, including (A) mean annual and (B) temporal variation (σ_{TAP} = 1 standard deviation) of $\delta^{18}O$ in tap water. Tap water supplies are classified as groundwater (circle), surface water (triangle), or managed water (square) (see Section 2.1). Names represent the city or town in which the site is located. Average values are shown from cites with multiple sites, including Tuscon, AZ, Davis, CA, San Diego, CA, Tallahassee, FL, Minneapolis, MN, and Houston, TX.

3. Results and discussion

3.1. Temporal variation

Annual average $\delta^{18}O$ values for the two sample years were very similar at a given site. Linear least-squares regression of the paired annual average values for 2005 and 2006 at 31 sites shows excellent correlation (1 standard error in parentheses): [$\delta^{18}O$, 2006] = 1.03(±0.02)[$\delta^{18}O$, 2005] + 0.4(±0.2), r^2 = 0.99. Year-on-year differences (Fig. 2) are slightly non-normally distributed (skewed right), a result confirmed at the 99% confidence level by application of the Lilliefors normality test ([34], p. 77–79). Although the specific controlling factors affecting the distribution of inter-annual range are not known, the skewness of the year-on-year distribution and the observation that 11 of these 14 surface water sites had mean annual values of $\delta^{18}O$ that were lower in 2005 than in 2006, together with a mean annual temperature for the contiguous USA that was 0.5 °C higher in 2006 than in 2005 (http://www.ncdc.noaa.gov/oa/climate/research/monitoring.html), suggests the possibility of climatological influences on tap water $\delta^{18}O$ values. By comparison, intra-annual range is, on average, ~4 times larger than inter-annual range (Fig. 3), suggesting that across

Table 1
Characteristics and isotopic values (annual averages and standard deviation in parentheses) for tap water supplies and local precipitation. All values are in units of ‰.

State/province	City	Type	$\delta^{18}O$	$\delta^{2}H$	$\delta^{18}O_{PPT}$	$\delta^{2}H_{PPT}$
Alberta	Lethbridge	SW	−17.2 (0.6)	−133 (4)	−15 (4.2)	−114 (31)
AZ	Tempe	MAN	−9.4 (0.7)	−75 (6)	−8.2 (2.2)	−62 (15)
AZ	Tucson1	GW	−8.3 (0.2)	−62 (2)	−8.6 (2.3)	−65 (15)
AZ	Tucson2	GW	−8.1 (0.5)	−60 (4)	−8.6 (2.3)	−65 (15)
CA	Berkeley	MAN	−11.1 (1.4)	−80 (10)	−9.6 (0.8)	−73 (6)
CA	Buena Park	MAN	−9.5 (0.7)	−72 (7)	−7.5 (0.8)	−60 (6)
CA	Davis1	GW	−8.1 (0.2)	−57 (2)	−9.8 (0.8)	−74 (5)
CA	Davis2	GW	−7.2 (0.3)	−51 (3)	−9.8 (0.8)	−74 (5)
CA	Fullerton	GW	−9.9 (0.4)	−77 (3)	−7.6 (0.8)	−61 (6)
CA	Pasadena	MAN	−8.7 (1.0)	−67 (9)	−8.1 (0.8)	−64 (6)
CA	SanDiego1	MAN	−9.7 (0.5)	−79 (4)	−7.2 (1.0)	−58 (7)
CA	SanDiego2	MAN	−9.7 (0.7)	−79 (5)	−7.2 (1.0)	−58 (7)
CO	Boulder	SW	−15.4 (1.2)	−116 (6)	−12.6 (3.0)	−94 (21)
FL	Tallahassee1	GW	−2.8 (0.2)	−16 (2)	−4.2 (1.1)	−26 (8)
FL	Tallahassee2	GW	−1.9 (0.2)	−11 (1)	−4.2 (1.1)	−26 (8)
FL	Tallahassee3	GW	−2.9 (0.2)	−16 (3)	−4.2 (1.1)	−26 (8)
GA	Athens	SW	−4.1 (0.5)	−24 (3)	−5.3 (2.5)	−33 (18)
GA	Watkinsville	GW	−5.2 (0.2)	−28 (2)	−5.4 (2.5)	−34 (18)
ID	Boise	MAN	−16.8 (0.3)	−129 (2)	−13 (2.4)	−98 (17)
IL	Chicago	SW	−5.8 (0.2)	−44 (2)	−7.7 (3.4)	−52 (24)
IL	Westmont	SW	−5.8 (0.2)	−45 (2)	−7.8 (3.4)	−53 (24)
IN	Evansville	SW	−7.4 (0.9)	−49 (5)	−6.5 (3.0)	−42 (22)
KS	Lawrence	SW	−3.7 (1.0)	−27 (6)	−7.5 (2.7)	−52 (19)
KS	Manhattan	GW	−5.4 (0.3)	−36 (2)	−7.8 (2.6)	−55 (18)
MD	Rockville	SW	−7.4 (0.4)	−48 (3)	−7.7 (3.0)	−49 (22)
MN	Minneapolis1	SW	−7.2 (1.0)	−56 (8)	−9.7 (3.8)	−69 (28)
MN	Minneapolis2	SW	−7.3 (1.1)	−56 (9)	−9.7 (3.8)	−69 (28)
MN	Wykoff	GW	−9.4 (0.2)	−63 (1)	−9.3 (3.6)	−65 (26)
NH	Durham	MAN	−8.2 (0.8)	−54 (6)	−9.7 (3.2)	−63 (24)
NM	Albuquerque	GW	−13 (0.2)	−97 (1)	−10.9 (2.4)	−77 (16)
NV	Las Vegas	SW	−11.8 (0.3)	−97 (2)	−9.8 (2.0)	−74 (12)
NV	Reno1	GW	−14.7 (0.2)	−109 (2)	−13 (2.2)	−97 (13)
NV	Reno2	MAN	−11.5 (1.6)	−88 (8)	−13 (2.2)	−97 (13)
NY	Ithaca	SW	−10.2 (1.0)	−69 (7)	−9.3 (3.2)	−61 (24)
OH	Columbus	SW	−7.7 (1.2)	−52 (7)	−7.7 (3.0)	−50 (22)
OR	Eugene1	GW	−10.2 (0.3)	−74 (2)	−11.3 (1.3)	−88 (9)
OR	Eugene2	SW	−11.9 (0.4)	−84 (3)	−11.3 (1.3)	−88 (9)
OR	Portland	SW	−10.4 (0.7)	−72 (6)	−11.3 (1.4)	−89 (9)
PA	University Park	GW	−9.3 (0.2)	−60 (1)	−8.9 (3.3)	−58 (23)
TX	Austin	SW	−1.8 (0.8)	−13 (5)	−4.4 (1.5)	−31 (9)
TX	Dallas	SW	−0.09 (1.0)	−2 (5)	−5.1 (1.6)	−36 (10)
TX	Houston1	SW	−2.0 (1.0)	−11 (5)	−3.8 (1.5)	−28 (9)
TX	Houston2	SW	−1.9 (1.0)	−11 (5)	−3.8 (1.5)	−28 (9)
UT	Salt Lake City	SW	−16 (0.3)	−120 (2)	−13.1 (2.6)	−97 (19)
VA	Great Falls	GW	−7.8 (0.2)	−47 (2)	−7.6 (3.0)	−48 (22)

GW: groundwater; SW: surface water; MAN: managed water; PPT: precipitation.

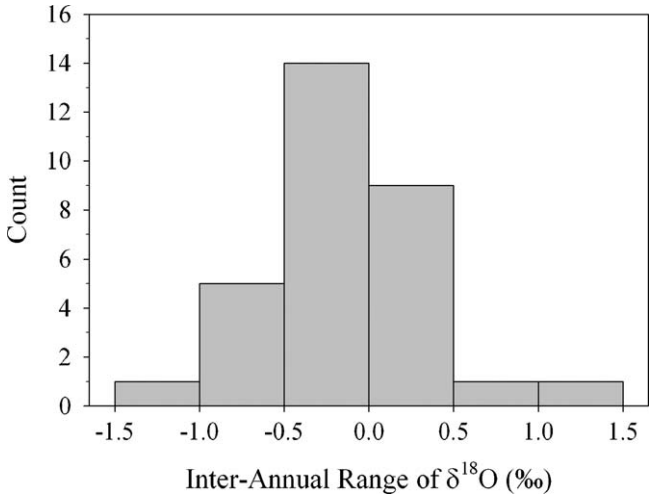

Fig. 2. Histogram of inter-annual range of $\delta^{18}O$ values of tap water, calculated as mean $\delta^{18}O$ from 2005 minus that from 2006.

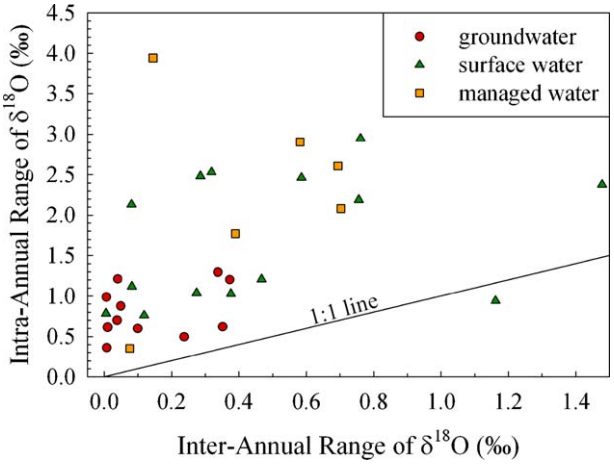

Fig. 3. Values of intra-annual range vs. inter-annual range for $\delta^{18}O$ in tap water.

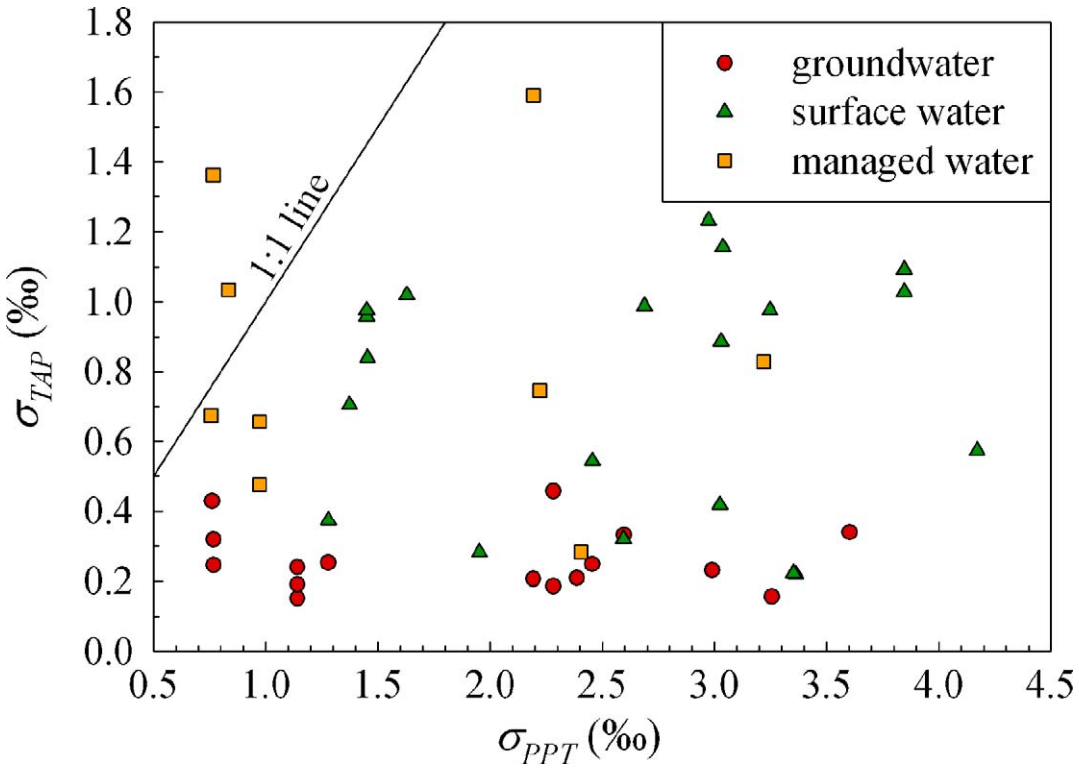

Fig. 4. Standard deviation (σ_{TAP}) of $\delta^{18}O$ values for monthly tap water samples and precipitation isotope ratio estimates (σ_{PPT}); circles, triangles, and squares represent tap water supplied by groundwater, surface water, and managed water, respectively.

the 2-year interval captured in our sample effort seasonal (monthly) variation of $\delta^{18}O$ in tap water represents a larger source of variability in the isotopic composition of human drinking waters than do longer-term (inter-annual) trends. Longer-term inter-annual variation in tap water $\delta^{18}O$ values remains unconstrained, however, and is worthy of additional study.

The $\delta^{18}O$ values of tap water supplies have been previously shown to vary geographically and temporally as the result of spatiotemporal variation in the isotopic composition of the precipitation from which these supplies are sourced [1]. Temporal variation in tap water $\delta^{18}O$ values (σ_{TAP}), however, is about 4× lower, on average, than that of precipitation (σ_{PPT}, Fig. 4). This difference can be attributed to the attenuation of short-term variations in precipitation water isotope ratios due to mixing surface-water and groundwater pools that are tapped by water supplies. Water-supply type was significantly correlated with values of σ_{TAP} (ANOVA, single factor, $p < 0.0001$), with relatively low values in groundwater supplies (average = 0.25‰, min. = 0.15‰, and max. = 0.46‰), high values in managed-water supplies (average = 0.85‰, min. = 0.28‰, and max. = 1.6‰), and

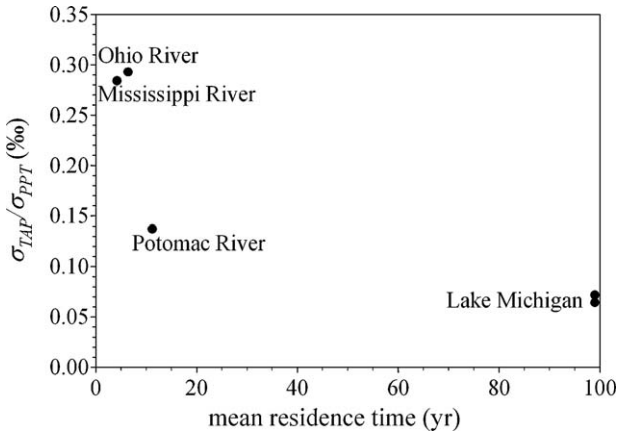

Fig. 5. Ratio of temporal variation in tap water and precipitation ($\sigma_{TAP}/\sigma_{PPT}$) vs. water residence time for selected surface water sites for which published values of residence time were available. Based on available data, values of $\sigma_{TAP}/\sigma_{PPT}$ (Table 1) and mean residence time are given for the Ohio River at Markland Dam, Kentucky [48] (about 280 km east of Evansville, IN), the Mississippi River at Anko, MN [49] (about 30 km north of Minneapolis, MN), the Potomac River at Point of Rocks, MD [49] (about 40 km northwest of Rockville), and Lake Michigan (http://www.epa.gov/glnpo/atlas/gl-fact1.html).

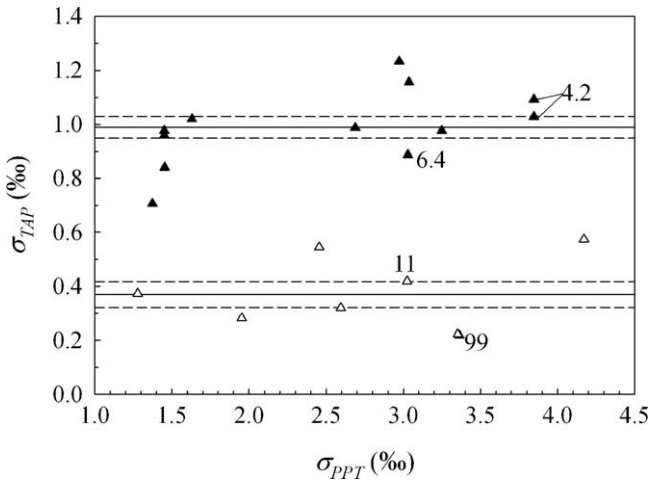

Fig. 6. Standard deviation (σ_{TAP}) of $\delta^{18}O$ values for the monthly surface water-supplied tap water samples and precipitation isotope ratio estimates (σ_{PPT}) in Fig. 4. Samples cluster into two groups (open vs. solid triangles), with average values of σ_{TAP} (solid lines) and one standard error (dashed lines) shown for each group. Parenthetical values give estimates of mean residence times (in years) based on published values for sites near Minneapolis, MN (4.2), Evansville, IN (6.4), Rockville, MD (11), and Westmont/Chicago, IL (99) (see Fig. 5 caption for further details on residence time values).

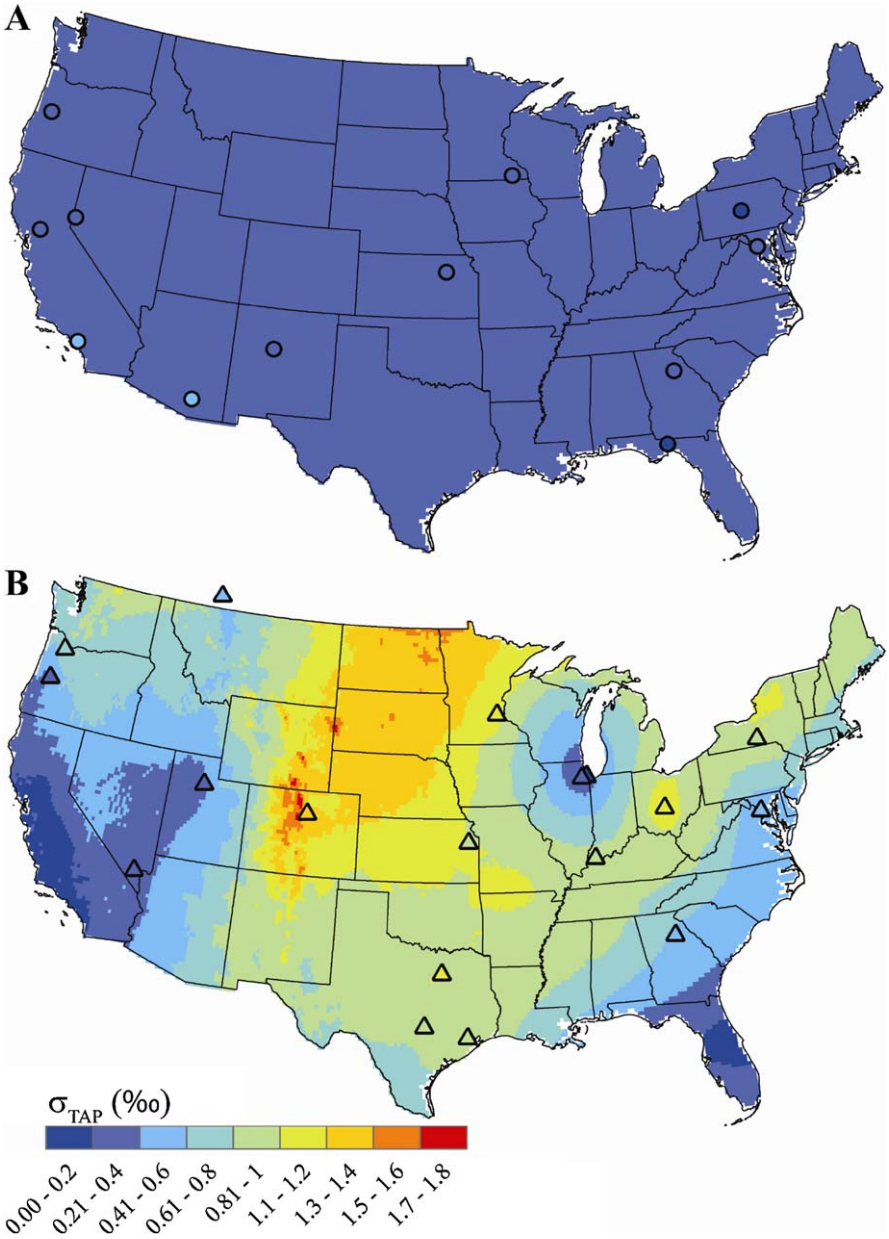

Fig. 7. Maps of temporal variation in $\delta^{18}O$ values of tap water supplied by groundwater (A) and surface water (B).

variable values in surface-water supplies (average = 0.74‰, min. = 0.22‰, and max. = 1.2‰).

For surface water supplies, our dataset provides evidence for the influence of both precipitation isotopic seasonality and attenuation during mixing on σ_{TAP} values. Values of σ_{TAP} are lower than those of σ_{PPT} at all surface water sites, and the highest values of tap water isotopic seasonality are found at sites with relatively high precipitation isotopic seasonality (Fig. 4). Estimates of mean residence time for selected surface water supplies sampled here range over 2 orders of magnitude, and in general are inversely related to the ratio $\sigma_{TAP}/\sigma_{PPT}$ (e.g., Fig. 5), a direct measure of the attenuation of the precipitation isotope variation in tap water supplies. This inverse relationship between water residence time and $\sigma_{TAP}/\sigma_{PPT}$ is likely at the root of the separation of surface values of $\sigma_{TAP}/\sigma_{PPT}$ into two groups, which have average values of 0.37‰ and 0.99‰ (ANOVA, single factor, $p < 0.0001$) and roughly corresponding to sites with long (years to decades) and short (few years) residence times (Fig. 6). Within the latter group values of σ_{TAP} exhibit a moderately strong correlation with σ_{PPT} ($p = 0.06$, F-test), further supporting the influence of precipitation isotope seasonality has on the intra-annual variation in tap water $\delta^{18}O$ values for sites with relatively short residence times.

Residence times for groundwaters are much longer than those for most surface water supplies [35–43], ranging from years to tens of millennia. Moreover, dispersion during the infiltration and flow of groundwater leads to significant mixing of waters, rapidly attenuating seasonal isotopic variability in most systems [44]. Within our dataset, groundwater-sourced tap water supplies show uniformly low values of σ_{TAP}, regardless of the magnitude of precipitation isotope seasonality (Figs. 1B and 4). This pattern is consistent with the ubiquitous attenuation of short-term (seasonal) isotopic variability during recharge and groundwater flow in all of the sampled systems.

The temporal dynamics of $\delta^{18}O$ in managed water are more complex than those of surface water or groundwater supplies, as they reflect not only environmental stresses but also the effects of

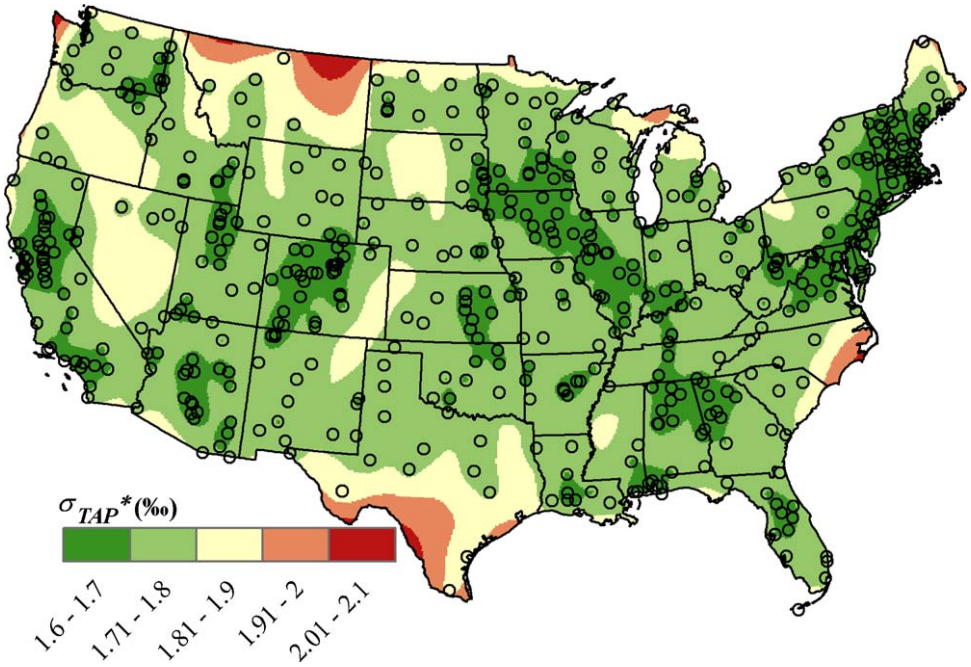

Fig. 8. Map of spatial interpolation uncertainty in $\delta^{18}O$ values of tap water from Bowen et al. [1]. Measurement locations of the $\delta^{18}O$ values of tap water are plotted as open circles.

active management of multiple water sources. For the one city where both groundwater and surface water supplies were sampled (Eugene, OR), the variation in $\delta^{18}O$ was significant (surface water $\delta^{18}O$ was −1.6‰ lower than groundwater (Table 1), consistent with a high-altitude runoff as a primary source of surface water). The potential exists for even larger variation in areas supplied by evaporated surface water or ancient groundwater, or where multiple water sources are used that originate from very different geographic locations (e.g., within much of the Metropolitan Water District of Southern California, where water is sourced from local precipitation, Colorado River water, and runoff from the Sierra Nevada Mountains). These differences may be manifested in the temporal patterns of $\delta^{18}O$ values in response to seasonal "switching" between supplies, leading to "artificial" seasonality in tap water $\delta^{18}O$ values. Within our dataset, σ_{TAP} values for several managed water supplies are similar to, or even higher than, values of σ_{PPT}, suggesting that active switching among water sources having different $\delta^{18}O$ values may have exaggerated the isotopic seasonality of these tap water supplies (Fig. 4, Table 1).

3.2. Geostatistical modeling

In order to develop spatially explicit maps of intra-annual variation in tap water $\delta^{18}O$ values that can be used to represent the range of natural seasonal variation around predicted mean values represented in tap water isoscapes, we investigated the spatial structure of σ_{TAP} values within our dataset. Spatial analysis indicates that values of σ_{TAP} are generally poorly clustered for groundwater, surface water, and managed water supplies (Table 2). With respect to groundwater supplies, this poor spatial clustering likely reflects the limited variation in values of σ_{TAP} (Fig. 1B). Given this, we suggest it is reasonable to approximate the seasonal variation in groundwater-derived tap waters using a fixed value of σ_{TAP} = 0.25‰ (the mean σ_{TAP} value for groundwater supplies in our data set) at all groundwater sites (Fig. 7A).

By comparison, values of σ_{TAP} for surface and managed water supplies span a wide range (Figs. 1B and 4). Although it is not statistically significant, visual inspection does suggest some geographic clustering of σ_{TAP} values for surface water supplies, with generally high values throughout the Great Lake, Midwest, and Gulf Coast regions, and low values along the eastern coast and western interior of the USA (Fig. 1B). Because the analysis presented in Section 3.1 suggested two independent controls on the seasonal variability of tap water derived from surface water sources (precipitation isotopic seasonality and residence time), we also attempted to isolate any spatial patterns in the σ_{TAP} values of surface water supplies by testing for spatial clustering of σ_{TAP} normalized by σ_{PPT} (i.e., $\sigma_{TAP}/\sigma_{PPT}$). In contrast to the result for the raw values of σ_{TAP}, the $\sigma_{TAP}/\sigma_{PPT}$ ratio showed significant, spatial clustering (Table 2). This clustering presumably reflects spatial patterns in the residence time and hydrology of surface water reservoirs related to regional variations in hydroclimate as well as regional differences in the demands on and management of surface water reservoirs.

In order to represent spatial variation in σ_{TAP} values we interpolated the observed values of $\sigma_{TAP}/\sigma_{PPT}$ onto a regular grid covering the contiguous USA and multiplied these values by gridded values of σ_{PPT}. The resultant map of σ_{TAP} for tap water derived from surface water supplies (Fig. 7B) shows a range of values from 0.12‰ to 1.8‰, with generally low values along both the eastern and western coasts of the USA and throughout the Rocky, Sierra, and Appalachian mountain ranges. The highest of these interpolated values (1.5–1.8‰) extend through the Dakotas, Minnesota, Kansas, Nebraska, and into portions of Colorado and Wyoming. Surface water supplies in the Great Lakes and Gulf Coast regions have intermediate levels of temporal variation, with interpolated values of σ_{TAP} ranging from 0.8‰ to 1.0‰.

Table 2
Moran's I test results and *Z* values for one standard deviation of tap water (σ_{TAP}), groundwater supplied tap water (σ_{GW}), surface water supplied tap water (σ_{SW}), managed water supplied tap water (σ_{MAN}), amount-weighted precipitation (σ_{PPT}), and the ratio of σ_{SW} to σ_{PPT} (σ_{SW}/σ_{PPT}).

Statistic	*I*	*Z*
σ_{TAP}	−0.01	0.09
σ_{GW}	−0.12	−0.20
σ_{SW}	0.26	1.44
σ_{MAN}	0	0.86
σ_{PPT}	−0.91	9.03
σ_{SW}/σ_{PPT}	1.02	5.04

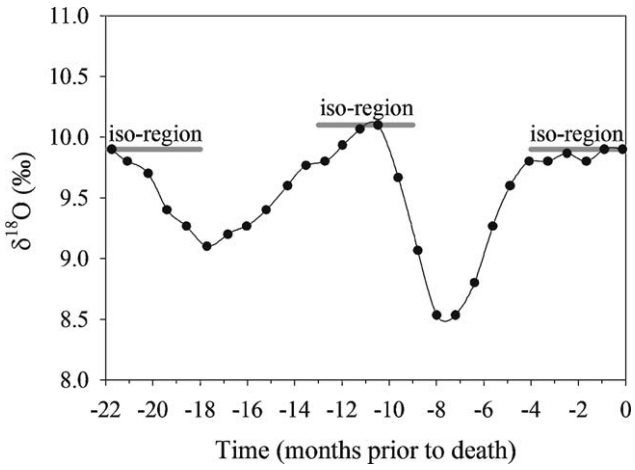

Fig. 9. Time sequence values of $\delta^{18}O$ measured from Saltair Sally before the victim's death [15]. Time was calculated based on an average hair growth rate of 0.4 mm day^{-1}. Ref. [15] identified three "iso-regions" that suggest locations where the victim resided prior to death. The three thick gray lines are used to identify the one of these three locations, "iso-region 1" [15], which is used in our analysis of geographic assignment.

Although analytical (measurement) error may contribute to uncertainty in the gridded surface in Fig. 7B, the dominant source of uncertainty in values of σ_{TAP} for surface water supplies is derived from the spatial interpolation of values of $\sigma_{TAP}/\sigma_{PPT}$. Using the semivariogram model in the Kriging interpolation method, a map of standard error for $\sigma_{TAP}/\sigma_{PPT}$ was generated and used to calculate interpolation uncertainty in values of σ_{TAP} for surface water supplies (i.e., maps of standard error for $\sigma_{TAP}/\sigma_{PPT}$ were added to average values of $\sigma_{TAP}/\sigma_{PPT}$, and then multiplied by the map of mean σ_{PPT} to yield a map of σ_{TAP} plus one standard error). One standard error for the gridded surfaces of σ_{TAP} (surface water) ranges from 0.06‰ to 0.98‰ (average = 0.37‰). The spatial distribution of standard error is controlled by sampling density, with the highest values (>0.5‰) occurring in poorly sampled parts of the northern Great Plains (e.g., Montana, North Dakota, South Dakota, Wyoming) and New England (Maine, New Hampshire, Vermont, Massachusetts, Rhode Island, Connecticut) and lowest values in proximity to sampling sites (average standard error at the 19 US sites is 0.13‰).

The newly created maps in Fig. 7A and B represent an incremental but important step toward characterizing temporal variation of $\delta^{18}O$ in managed water supplies, which may serve the largest number of individuals in the western USA (Fig. 1A). Temporal variation in $\delta^{18}O$ values of managed water can be viewed as a function (1) the isotopic variability in the groundwater and surface water supplies that compose local managed water and (2) the human–managed interaction between these supplies in response supply and demand. The results presented here suggest that the isotope variation in local precipitation and water supply residence time are the primary determinants of temporal variation of $\delta^{18}O$ in groundwater and surface water supplies, which will add to future work on the dynamics of multiple active water supplies, but is not considered further or in our analysis of geographic assignment.

3.3. Spatial interpolation uncertainty

Uncertainty in the predicted mean $\delta^{18}O$ values of tap water ($\sigma_{TAP}{}^{*}$) varies as a function of proximity to tap water sampling sites (Fig. 8). Values of $\sigma_{TAP}{}^{*}$ range from 1.6‰ to 2.1‰ (average = 1.8‰), with 97% (by area) of the contiguous USA having values between 1.6‰ and 1.9‰ (Fig. 8). The highest values of $\sigma_{TAP}{}^{*}$ (>2.0‰) occur locally in portions of southwest Texas and northern Minnesota. By comparison values of $\sigma_{TAP}{}^{*}$ are less variable but larger in magnitude than the interpolated values of σ_{TAP} for surface water, with the ratio between the two ($\sigma_{TAP}{}^{*}/\sigma_{TAP}$) ranging from 0.97 to 14 (0.02% of the grid cells have $\sigma_{TAP}{}^{*}/\sigma_{TAP} < 1$). Although values of σ_{TAP} represent a significant component of uncertainty in geographic assignment of human hair, other sources of uncertainty, such as $\sigma_{TAP}{}^{*}$, can be as large (or larger). Our analysis highlights the need to improve our understanding of the mechanisms driving local-scale spatial distributions of $\delta^{18}O$ in tap water.

3.4. Likelihood-based assignment

Temporal variation and spatial interpolation uncertainty in $\delta^{18}O$ values of tap water were evaluated with respect to their effects on the geographic assignment of human hair from the remains of an unidentified woman found in Saltair, Utah, referred to in the literature (e.g., [15]) and by law enforcement officials as "Saltair Sally". As described in [15], the case of Saltair Sally involves the discovery of the decomposed, scattered remains of a young female, approximately 17–20 years of age, in October 2000. The remains were found in a shallow grave and consisted of several personal effects, the cranium and teeth, and the intact strands of the victim's scalp hair. Local law enforcement was able to reconstruct the time since death (approximately 12–24 months), but efforts to verify the victim's identity were unsuccessful. In 2007, the Utah State Medical Examiner released a ~26-cm long sample the victim's hair for isotope ratio analysis. Values of $\delta^{18}O$ determined using established methods at IsoForensics, Inc. (http://www.isoforensics.com) [6,45] varied sequentially along the strand of hair, suggesting that the victim had traveled to three isotopically distinct locations over the 2 years prior to death (Fig. 9). In our analysis of geographic assignment we consider one of the apparent locations, defined based on the $\delta^{18}O$ value of 10‰ (hair) which occurred recurrently over the length of hair and which may correspond with a geographic location to which the victim returned repeatedly including immediately prior to death. This particular iso-location is evident at three distinct time intervals (Fig. 9), with a standard deviation of these values equal to ±0.1‰ and within the 0.2‰ analytical precision of the hair isotope measurement. A full discussion of other sources of uncertainty in the geographic assignment of $\delta^{18}O$ human scalp hair (e.g., changes in diet, regression transformation from water to hair $\delta^{18}O$) is beyond the scope of this paper, but it is worth noting that these factors may contribute to geographic variation in hair $\delta^{18}O$.

Maps representing the likelihood of origin for the observed hair $\delta^{18}O$ value of 10‰ were generated using an isoscape of predicted average hair $\delta^{18}O$ values [6] and 4 distinct sets of assumptions about the uncertainty of the isoscape values: (1) uncertainty in the hair isoscape values (σ_i) is equal to the intra-annual isotopic variation in groundwater supplies (Fig. 10A), (2) σ_i is equal to the intra-annual isotopic variation in surface water supplies (Fig. 10B), (3) σ_i is equal to the combination of uncertainty in scenario (1) plus spatial interpolation uncertainty (Fig. 10C), and (4) σ_i is equal to the combination of uncertainty in scenario (2) plus spatial interpolation uncertainty (Fig. 10D). On each map all likelihood surfaces are rescaled relative to the largest likelihood value to yield a relative scale ranging from 0 to 1. Although this rescaling allows for comparison of the distribution of likelihood values within and among each of the 4 scenarios, it precludes quantitative point-to-point comparison among the maps. The results presented here, therefore, focus on the geographic distribution of the gridded likelihood values.

For each of the 4 scenarios, the spatial distribution of likelihood values is consistent with the western USA as the region of origin for Saltair Sally, with the distribution of high likelihood values largely

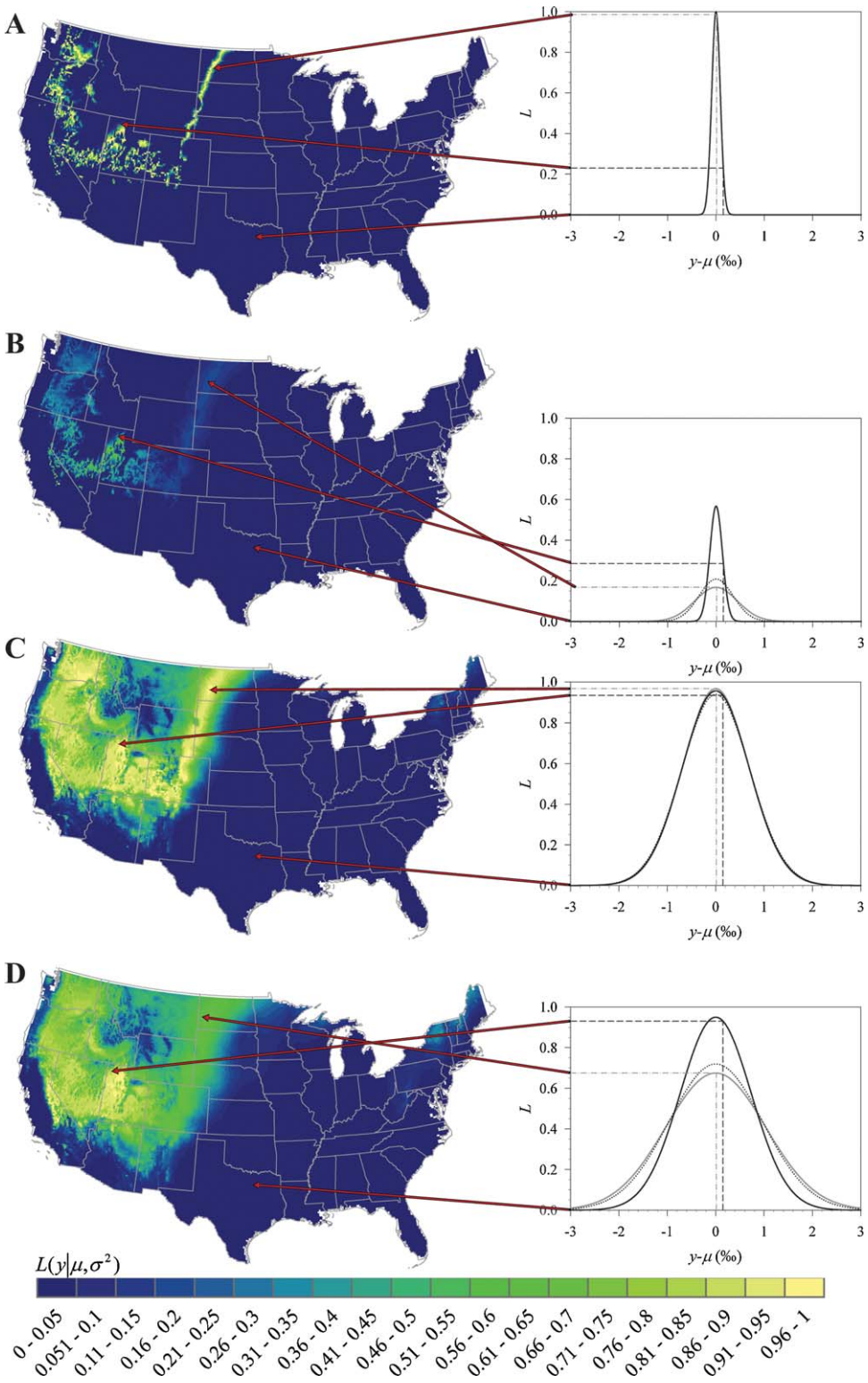

Fig. 10. Maps of likelihood-based geographic assignment assuming (A) uncertainty in the hair isoscape values (σ_i) equal to the intra-annual isotopic variation in groundwater supplies (Fig. 7A), (B) σ_i is equal to the intra-annual isotopic variation in surface water supplies (Fig. 7B), (C) σ_i is equal to the combination of intra-annual isotopic variation in groundwater supplies (Fig. 7A) plus spatial interpolation uncertainty (Fig. 8), and (D) σ_i is equal to the combination of intra-annual isotopic variation in surface water supplies (Fig. 7B) plus spatial interpolation uncertainty (Fig. 8). The distribution of possible likelihood values for three grid cells is displayed to the right of the maps, with sites located in Utah (black solid and dashed line), North Dakota (gray solid and dashed lines), and Texas (black dotted line). Red arrows point to the locations of the sites and corresponding likelihood values (L). Note that values of $y - \mu$ (difference between measured and predicted hair $\delta^{18}O$) are +5‰ for the Texas grid cell (not shown on x-axis) and correspond to values of L equal to 0. (For interpretation of the references to colour in this figure legend, the reader is referred to the web version of the article.)

restricted to the western interior region (Fig. 10). The areal extent of high likelihood values throughout the western USA differs substantially among the scenarios, however, with likelihood values equal to or greater than 0.95 representing an area of 82,472 km^2; 263 km^2; 92,715 km^2; and 26,528 km^2 for scenarios 1–4, respectively. The geographic distribution of high likelihood values ($L \geq 0.95$) spans 12 states (Washington, Oregon, Idaho, California, Nevada, Utah, Colorado, New Mexico, Wyoming, Nebraska, South Dakota, and North Dakota) for scenario 1, 1 state (California) for scenario 2, 10 states (Arizona and 9 of the 12 states for scenario 1) for scenario 3, and 3 states (California, Nevada, and Utah) for scenario 4. The disparity among these areal coverages implies that the adoption of different assumptions about uncertainty and temporal variation in tap water isotope ratios can lead to contrasting interpretations of the strength and specificity of geographic assignment of human scalp hair isotope ratios. However, despite these discrepancies, the 4 scenarios all effectively rule out ~99% (by area) of the contiguous USA as a likely ($L = 0.95$) location of origin for Saltair Sally. Confining the region of origin to a relative small percentage of the contiguous USA represents an informative piece of forensic evidence in this case.

Equally as informative, particularly with respect to the future development and refinement of isotope-based geographic assignment techniques, is an analysis of the factors contributing to the differences in the gridded likelihood surfaces (Fig. 10A–D). These geographic distributions reflect the isotopic separation between measured and modeled average $\delta^{18}O$ values of hair ($y - \mu_i$), which is constant for any given location across all scenarios, and the values of σ_i,, which govern the distribution of possible likelihood values (i.e., the probability density function) for a given value of $y - \mu_i$. If values of σ_i are assumed spatially constant (i.e., scenario 1), then the distribution of possible likelihood values does not vary spatially and, accordingly, the resulting likelihood surfaces are a function of $y - \mu_i$ (Fig. 10A). For scenario 1, where only the relatively small uncertainty related to temporal variation in ground water $\delta^{18}O$ values is considered, the distribution of likelihood values is constrained to a very narrow region and only a relatively small number of locations with values of y very close to μ_i are considered highly likely locations of origin. Such values of y are distributed throughout the western USA, however, such that the likely location of origin, while very specific in terms of the spatial area having high likelihood, includes likely origins in many different states. If a larger (or smaller) value was assumed for the temporal variation in groundwater $\delta^{18}O$, the effect would be to increase (or decrease) the areal extent of high-likelihood values (e.g., the geographic area with $L \geq 0.95$ expands by a factor of ~2 when σ_{TAP} is increased from 0.25‰ to 0.50‰) without affecting the spatial distribution of the locations of maximum L.

Under each of the other scenarios the values of σ_i vary geographically, meaning that the value of L at a given cell relative to others depends on both $y - \mu_i$ and σ_i. Grid cells with relatively high values of σ_i give flattened/widened distributions of possible likelihood values and, consequently, comparatively lower peak likelihood values and higher tail likelihood values. This point is best illustrated in Fig. 10B, which shows the likelihood value distributions for sites in North Dakota and Utah with substantially different values of $y - \mu_i$ (0.015‰ vs. 0.15‰) and σ_i (0.43‰ vs. 0.13‰), respectively. The higher likelihood value occurs at the Utah site, not because $y - \mu_i$ is closer to zero, but because the value of σ_i is lower at that site.

Likelihood ratios are a common and accepted metric for use in hypothesis tests of the source of evidentiary material ([46,47]), and many disciplines are moving toward likelihood ratios (and away from probability surfaces) as the *de facto* standard for evaluation of scientific evidence. The calculated likelihood surfaces in Fig. 10 provide a unique opportunity to assess the likelihood ratio (LR) of geographic origin between any two locations (L_1 and L_2):

$$LR = \frac{P(L_1)}{P(L_2)} \quad (4)$$

Eq. (4) provides a quantitative assessment of the degree of support for L_1 vs. L_2, with values of LR greater than 1 supporting L_1, values of less than 1 supporting L_2, and values close to 1 suggesting no preference for either L_1 or L_2. As an illustration of this application, we use equation (4) to evaluate the relative probability of geographic origin among three locations in Utah (UT), North Dakota (ND), and Texas (TX). Using the likelihood values in Fig. 10, values of LR were calculated for L_1 = UT vs. L_2 = ND, L_1 = UT vs. L_2 = TX, and L_1 = ND vs. L_2 = TX, with results yielding LR values that strongly support ($LR > 1000$) both UT and ND as the more probable locations of origin than TX (Table 3). However, the case of UT vs. ND results in values of LR closer to 1, suggesting that it is not be feasible to distinguish between these locations of origin based on the isotopic data. The likelihood ratio approach as applied to geographic assignment using stable isotope data warrants further investigation, but we note here that it represents a powerful approach both for hypothesis testing and for assessment of methodological strength. For example, although our analysis reported above clearly shows that different uncertainty assumptions have large effects on isotope-based geographic assignment maps, the likelihood ratio analysis suggests that for questions involving the three locations investigated here the method is largely insensitive to the assumed uncertainty models tested here.

Table 3
Likelihood ratios for single grid cells located in northern Utah (UT), North Dakota (ND), and Texas (TX) (Fig. 10). Likelihood ratios are shown for the 4 different scenarios used to structure σ (see Section 3.4).

	Likelihood ratio ($LR = L_1/L_2$)		
	L_1 = UT, L_2 = ND	L_1 = UT, L_2 = TX	L_1 = ND, L_2 = TX
Scenario 1	4	>1000	>1000
Scenario 2	1	>1000	>1000
Scenario 3	1	>1000	>1000
Scenario 4	1	>1000	>1000

4. Conclusions

Hydrologic monitoring of tap water stable isotope ratios during a two-year period reveals spatially explicit patterns of temporal variation in $\delta^{18}O$ values of tap water across the contiguous USA. These patterns can be related to inherent differences in the physical and hydrological water-supply characteristics, including variations in water residence times and seasonality of local precipitation $\delta^{18}O$. Although local hydroclimatological factors (e.g., lake recycling, surface water evaporation, etc.) may also influence the temporal dynamics of $\delta^{18}O$ in tap water, robust spatial gradients of σ_{TAP} (at least for non-managed water supplies) are largely related to regional patterns of precipitation isotopic seasonality modulated by water residence time. Based on this relationship, geostatistical models were developed and used to create geographic representations (i.e., maps) of σ_{TAP} values (Fig. 7A and B). These maps are a first of their kind and document an important hydroclimatological source of uncertainty in geographic assignment of human hair.

Applying these maps (Fig. 7A and B) to geospatial forensic investigations, we explored the effects of temporal variation and spatial interpolation uncertainty in $\delta^{18}O$ values of tap water on retrospective geographic assignment of scalp hair from the

remains of an unidentified woman found in Saltair, Utah. Although assumptions regarding the source of uncertainty (temporal vs. spatial interpolation; groundwater vs. surface water) have only a modest effect on assignment of region-of-origin over large spatial scales, they may influence geographic assignment questions involving comparisons at more local (e.g., within-state) spatial scales. This effect is clear in comparison of likelihood-of-origin maps that include the combined effects of temporal variation and spatial interpolated uncertainty to those that are based on temporal variation alone (e.g., Fig. 10A vs. Fig. 10B). For any assignment question, the relative strength of the geographic variation in $\delta^{18}O$ values of hair and the temporal/geostatistical variation in these values ultimately dictates the strength of assignment. Although our analysis clearly indicates cases in which the strength of geographic assignment will be influenced by temporal variation and interpolation uncertainty in tap water $\delta^{18}O$, our results indicate that, even when constrained by multiple sources of uncertainty, human scalp hair is isotopically distinct on a regional scale in the USA.

Acknowledgements

We acknowledge the financial support of this work by the US federal government and by IsoForensics, Inc. We are sincerely grateful to the countless individuals that have contributed tap water samples to this project.

References

[1] G.J. Bowen, et al., Stable isotope ratios of tap water in the contiguous USA, Water Resources Research 43 (2007) W03419.
[2] A. Dutton, et al., Spatial distribution and seasonal variation in $^{18}O/^{16}O$ of modern precipitation and river water across the conterminous United States, Hydrological Processes 19 (2005) 4121–4146.
[3] J.R. Gat, Lakes, in: J.R. Gat, R. Gonfiantini (Eds.), Stable Isotope Hydrology: Deuterium and Oxygen-18 in the Water Cycle. Technical Report Series No. 210, IAEA, Vienna, 1981, pp. 203–221.
[4] C. Kendall, T.B. Coplen, Distribution of oxygen-18 and deuterium in river waters across the United States, Hydrological Processes 15 (7) (2001) 1363–1393.
[5] G.I. Smith, et al., Stable isotope compositions of waters in the Great Basin, United States 3. Comparison of groundwaters with modern precipitation, Journal of Geophysical Research 107 (2002) 4402 (D19) doi: 10.1029/2001JD000567.
[6] J.R. Ehleringer, et al., Hydrogen and oxygen isotope ratios in human hair are related to geography, Proceedings of the National Academy of Sciences of the United States of America 105 (8) (2008) 2788–2793.
[7] G.J. Bowen, et al., Stable hydrogen and oxygen isotope ratios of bottled waters of the world, Rapid Communications in Mass Spectrometry 19 (2005) 3442–3450.
[8] L.A. Chesson, et al., Links between purchase location and stable isotope ratios of bottled water: soda, and beer in the United States, Journal of Agricultural and Food Chemistry 58 (12) (2010) 7311–7316.
[9] L.A. Chesson, et al., Hydrogen and oxygen stable isotope ratios of milk in the United States, Journal of Agricultural and Food Chemistry 58 (4) (2010) 2358–2363.
[10] G.J. Bowen, et al., Dietary and physiological controls on the hydrogen and oxygen isotope ratios of hair from mid-20th century indigenous populations, American Journal of Physical Anthropology 139 (2009) 494–504.
[11] I. Fraser, W. Meier-Augenstein, R.M. Kalin, The role of stable isotopes in human identification: a longitudinal study into the variability of isotopic signals in human hair and nails, Rapid Communication in Mass Spectrometer 20 (7) (2006) 1109–1116.
[12] T.C. O'Connell, R.E.M. Hedges, Isotopic comparison of hair and bone: archaeological analyses, Journal of Archaeological Science 26 (1999) 661–665.
[13] Z.D. Sharp, et al., Hydrogen isotope systematics of hair: archeological and forensic applications, Journal of Archaeological Science 30 (2003) 1709–1716.
[14] A.H. Thompson, et al., Stable isotope analysis of modern human hair collected from Asia (China: India, Mongolia, and Pakistan), American Journal of Physical Anthropology 141 (3) (2009) 440–451.
[15] J.R. Ehleringer, et al., A framework for the incorporation of isotopes and isoscapes in geospatial forensic investigations, in: J.B. West, et al. (Eds.), Isoscapes: Understanding Movement, Pattern, and Process on Earth Through Isotope Mapping, Springer, New York, 2010, pp. 357–387.
[16] W. Meier-Augenstein, I. Fraser, Forensic isotope analysis leads to identification of a mutilated murder victim, Science & Justice 48 (3) (2008) 153–159.
[17] M.B. Wunder, D.R. Norris, in: K.A. Hobson, L.I. Wassenaar (Eds.), Analysis and Design for Isotope-based Studies of Migratory Animals. Tracking Animal Migration with Stable Isotopes, 2008.
[18] M.B. Wunder, Using isoscapes to model probability surfaces for determining geographic origins, in: G.J. Bowen, et al. (Eds.), Isoscapes: Understanding Movement, Pattern, and Process of Earth Through Isotope Mapping, Springer, New York, 2010, pp. 251–270.
[19] K.A. Hobson, Tracing origins and migration of wildlife using stable isotopes: a review, Oecologia 120 (3) (1999) 314–326.
[20] K.A. Hobson, Stable isotopes and the determination of avian migratory connectivity and seasonal interactions, Auk 122 (4) (2005) 1037–1048.
[21] D.R. Rubenstein, K.A. Hobson, From birds to butterflies: animal movement patterns and stable isotopes, Trends in Ecology & Evolution 19 (5) (2004) 256–263.
[22] M.B. Wunder, et al., A test of geographic assignment using isotope tracers in feathers of known origin, Oecologia 144 (2005) 607–617.
[23] K.A. Hobson, et al., A method for investigating population declines of migratory birds using stable isotopes: origins of harvested lesser scaup in North America, PLoS One 4 (11) (2009).
[24] C.A. Lott, J.P. Smith, A geographic-information-system approach to estimating the origin of migratory raptors in North America using stable hydrogen isotope ratios in feathers, Auk 123 (3) (2006) 822–835.
[25] D.R. Norris, et al., Migratory connectivity of a widely distributed songbird, the American Redstart (Setophaga ruticilla), Ornithological Monographs 61 (2006) 14–28.
[26] J.A. Royle, D.R. Rubenstein, The role of species abundance in determining breeding origins of migratory birds with stable isotopes, Ecological Applications 14 (6) (2004) 1780–1788.
[27] M.B. Wunder, D.R. Norris, Improved estimates of certainty in stable-isotope-based methods for tracking migratory animals, Ecological Applications 18 (2) (2008) 549–559.
[28] T.B. Coplen, New guidelines for reporting stable hydrogen: carbon, and oxygen isotope-ratio data, Geochimica et Cosmochimica Acta 60 (17) (1996) 3359–3360.
[29] G.J. Bowen, J. Revenaugh, Interpolating the isotopic composition of modern meteoric precipitation, Water Resources Research 39 (2003) 1299.
[30] G.J. Bowen, L.I. Wassenaar, K.A. Hobson, Global application of stable hydrogen and oxygen isotopes to wildlife forensics, Oecologia 143 (3) (2005) 337–348.
[31] G.J. Bowen, B. Wilkinson, Spatial distribution of $\delta^{18}O$ in meteoric precipitation, Geology 30 (4) (2002) 315–318.
[32] N.L. Ingraham, B.E. Taylor, Light stable isotope systematics of large-scale hydrologic regimes in California and Nevada, Water Resources Research 27 (1) (1991) 77–90.
[33] C. Cressie, Statistics for Spatial Data, John Wiley and Sons, New York, 1993, 900.
[34] P. Sprent, Applied Nonparametric Statistical Methods, 2nd ed., Chapman and Hall, 1993,, p. 340.
[35] W. Aeschbach-Hertig, et al., A paleotemperature record derived from dissolved noble gases in groundwater of the Aquia Aquifer (Maryland: USA), Geochimica Et Cosmochimica Acta 66 (5) (2002) 797–817.
[36] E. Busenberg, L.N. Plummer, Use of chlorofluorocarbons (Ccl3f And Ccl2f2) as hydrologic tracers and age-dating tools—the alluvium and terrace system of central Oklahoma, Water Resources Research 28 (9) (1992) 2257–2283.
[37] S.A. Dunkle, et al., Chlorofluorocarbons (Ccl3f And Ccl2f2) as dating tools and hydrologic tracers in shallow groundwater of the Delmarva Peninsula: Atlantic coastal-plain, United-States, Water Resources Research 29 (12) (1993) 3837–3860.
[38] C.D. Kennedy, D.P. Genereux, C-14 groundwater age and the importance of chemical fluxes across aquifer boundaries in confined cretaceous aquifers of North Carolina: USA, Radiocarbon 49 (3) (2007) 1181–1203.
[39] C.D. Kennedy, et al., Relationships among groundwater age, denitrification, and the coupled groundwater and nitrogen fluxes through a streambed, Water Resources Research 45 (2009).
[40] P.B. McMahon, J.K. Bohlke, S.C. Christenson, Geochemistry: Radiocarbon ages, and paleorecharge conditions along a transect in the central high plains aquifer, southwestern Kansas, USA, Applied Geochemistry 19 (11) (2004) 1655–1686.
[41] E. Modica, H.T. Burton, L.N. Plummer, Evaluating the source and residence times of groundwater seepage to streams: New Jersey Coastal Plain, Water Resources Research 34 (11) (1998) 2797–2810.
[42] L.N. Plummer, et al. Geochemical characterization of ground-water flow in the Santa Fe Group Aquifer system, Middle Rio Grande Basin, New Mexico, in: Water-Resources Investigations Report 03-4131. 2004, USGS. p. 396.
[43] L.N. Plummer, C.L. Sprinkle, Radiocarbon dating of dissolved inorganic carbon in groundwater from confined parts of the Upper Floridan aquifer: Florida, USA, Hydrogeology Journal 9 (2) (2001) 127–150.
[44] C.J. Barnes, G.B. Allison, Tracing of water movement in the unsaturated zone using stable isotopes of hydrogen and oxygen, Journal of Hydrology 100 (1-3) (1988) 143–176.
[45] G.J. Bowen, et al., Treatment methods for the determination of δ^2H and $\delta^{18}O$ of hair keratin by continuous-flow isotope-ratio mass spectrometry, Rapid Communications in Mass Spectrometry 19 (2005) 2371–2378.
[46] N. Farmer, W. Meier-Augenstein, D. Lucy, Stable isotope analysis of white paints and likelihood ratio, Science & Justice 49 (2009) 114–120.
[47] G. Pierrini, et al., Evaluation of preliminary isotopic analysis (13C and 15N) of explosives: a likelihood ratio of approach to assess the links between semtex samples, Forensic Science International 167 (2007) 43–48.
[48] R.L. Michel, Tritium hydrology of the Mississippi River basin, Hydrological Processes 18 (7) (2004) 1255–1269.
[49] R.L. Michel, Residence times in river basins as determined by analysis of long-term tritium records, Journal of Hydrology 130 (1–4) (1992) 367–378.